

Calculation of multiphoton ionization amplitudes and cross sections of few-electron atoms

Andrej Mihelič*

*Jožef Stefan institute, Jamova cesta 39, SI-1000 Ljubljana, Slovenia and
Faculty of mathematics and physics, University of Ljubljana, Jadranska ulica 19, SI-1000 Ljubljana, Slovenia*

Martin Horvat†

*Faculty of mathematics and physics, University of Ljubljana, Jadranska ulica 19, SI-1000 Ljubljana, Slovenia
(Dated: March 31, 2021)*

We present a theoretical method for calculating multiphoton ionization amplitudes and cross sections of few-electron atoms. The present approach is based on an extraction of partial wave amplitudes from a scattering wave function, which is calculated by solving a system of driven Schrödinger equations. The extraction relies on a description of partial waves in terms of a small number of Coulomb waves with fixed wave numbers. The method can be used for photon energies below and above the ionization threshold and to treat resonance-enhanced multiphoton ionization. We use it to calculate two-, three-, and four-photon ionization cross sections of hydrogen and helium atoms for a wide range of photon energies and to determine the asymmetry parameters of photoelectron angular distributions for two-, three-, and four-photon ionization of the helium atom.

I. INTRODUCTION

Theoretical treatment of multiphoton ionization, specifically, calculation of multiphoton ionization rates and cross sections, has been a recurring topic since the early experiments on multiphoton ionization [1, 2]. It remains an important subject of recent theoretical and experimental studies based on free electron laser (FEL) and high-order harmonic generation (HHG) sources [3–7]. Calculations of multiphoton ionization amplitudes and cross sections are particularly demanding when describing a process in which one or several photons are absorbed at energies above the ionization threshold (above threshold ionization, ATI). When this is the case, dealing with continuum-continuum transitions can not be avoided. The presence of resonance (quasi-bound) states which are embedded in the continua makes the theoretical description even more demanding; ionization rates may be seen to be strongly modified when the photon energy lies close to a resonance, either in the intermediate step (resonance enhanced multiphoton ionization, REMPI) or the final step of a multiphoton process.

Over the last two decades, a theoretical description based on exterior complex scaling (ECS) seems to have gained momentum. Using the ECS approach, one is able to efficiently describe both resonant and nonresonant continuum. As will be discussed, the ECS method is based on a complex transformation of radial (electronic) coordinates outside a sphere of a given radius (see Ref. [8] and the references therein). This allows one to calculate transition (scattering, ionization) amplitudes from the part of the wave function which is contained inside the unmodified region of the coordinate space. Theoret-

ical methods used in these calculations resemble those used with bound (localized) states and real, square integrable basis sets. Methods based on ECS have been used to calculate one- and two-photon single and double photoionization cross sections [9–12]. ECS has also been used to study electron dynamics of atoms and simple molecules driven by short, intense pulses. The complex coordinate transformation prevents artifacts which originate from the reflections of the wave packet on the boundaries of the simulation volume, and thus eliminates the need for special approaches, such as complex absorbing potentials (CAPs) [13]. A very elegant method based on ECS was used by Palacios *et al.* [14–17] to extract partial ionization amplitudes and cross sections from the wave packet. A particularly efficient implementation of the ECS method, the infinite-range complex scaling (irECS) [13], was combined with the time-dependent surface flux approach (tSurff) [18, 19] to solve the time-dependent Schrödinger equation in minimal simulation volumes. It was used in combination with the time-dependent complete-active-space self-consistent method [20] to study strong-field ionization and high-order harmonic generation in He, Be, and Ne atoms [21].

Despite the apparent shift in interest in the recent years from the time-independent to the time-dependent treatment of multiphoton processes, many experiments exist for which solving the time-dependent Schrödinger equation may not be feasible, for example, when the pulse duration exceeds a few tens of femtoseconds. In these cases, reliable (multiphoton) ionization cross sections are a valuable and efficient means of assessing the ionization probabilities.

In this work, we describe an efficient method for the calculation of multiphoton ionization amplitudes and cross sections which is based on the time-independent perturbation theory and is applicable in the case of a single electron ejection. We use it to calculate generalized two-, three- and four-photon cross sections of the ground-

* andrej.mihelic@ijs.si

† martin.horvat@fmf.uni-lj.si

state hydrogen and helium atoms for a wide range of photon energies. Furthermore, we calculate the asymmetry parameters which are used to characterize photoelectron angular distributions in the case of two-, three- and four-photon ionization of helium. To our knowledge, calculations of neither the higher-order cross sections of helium in the ATI energy region nor the asymmetry parameters for multiphoton ionization exist in the literature.

II. PARTIAL IONIZATION AMPLITUDES AND CROSS SECTIONS

The discussion in this section is divided into two parts. In Section II A, we briefly review the formalism used to calculate transition amplitudes for one-photon ionization. In Section II B, we show how the formalism can be modified to be applicable for two- and multiphoton ionization. The method we present here is based on the approach used in Refs. [9, 11, 22, 23] to calculate ionization amplitudes for double electron ejection and extends on the work described in Ref. [12]. Hartree atomic units are used throughout this work unless stated otherwise.

A. One-photon ionization

Let us write the total Hamiltonian operator of an N -electron atom as $H = H_f + V_f$, where H_f denotes the channel Hamiltonian operator and V_f the short-range perturbation. The choice of H_f defines the final-state (post-collision) arrangement channels [24]. We describe the photoionization process in terms of the channel wave functions (Φ_f), which are eigen wave functions of H_f at specific energy E above the ionization threshold,

$$H_f \Phi_f = E \Phi_f. \quad (1)$$

Next, let D denote the dipole transition operator and let Ψ_0 be an eigen wave function of H with energy E_0 which describes the initial (bound) atomic state. As we describe below, the partial ionization amplitudes may be calculated from the solution of a driven time-independent Schrödinger equation,

$$(E - H) \hat{\Psi} = D \Psi_0, \quad (2)$$

where $E = E_0 + \omega$ and ω denotes the photon energy.

We write the total and channel Hamiltonian operators as $H = T + W$ and $H_f = T + W_f$, where $T = -\nabla^2/2$ is the kinetic energy operator and $\nabla = (\nabla_1, \dots, \nabla_N)$ is the multidimensional gradient operator. We use these forms to rewrite Eq. (2) and the complex conjugate of Eq. (1) as:

$$\left\{ E + \frac{\nabla^2}{2} - W \right\} \hat{\Psi} = D \Psi_0, \quad (3)$$

$$\left\{ E + \frac{\nabla^2}{2} - W_f \right\} \Phi_f^* = 0, \quad (4)$$

where the asterisk denotes complex conjugation. By multiplying Eqs. (3) and (4) with Φ_f^* and $\hat{\Psi}$, respectively, subtracting the results, and integrating over volume \mathcal{V} (a $3N$ -dimensional manifold) in which V_f is non-negligible, we obtain the following relation:

$$\begin{aligned} & \langle \Phi_f | D | \Psi_0 \rangle_{\mathcal{V}} + \langle \Phi_f | V_f | \hat{\Psi} \rangle_{\mathcal{V}} \\ &= \frac{1}{2} \int_{\mathcal{V}} d\tau \{ \Phi_f^* \nabla^2 \hat{\Psi} - \hat{\Psi} \nabla^2 \Phi_f^* \}. \end{aligned} \quad (5)$$

We have taken into account that $W - W_f = H - H_f = V_f$ and used a subscript to denote integration over \mathcal{V} . In this section, we assume that the integration volume is large enough, so that the magnitude of the square-integrable driving term ($D\Psi_0$) is negligibly small outside volume \mathcal{V} . We will return to this point in Section II B. The expression in the curly brackets in Eq. (5) is equal to $\nabla \cdot \{ \Phi_f^* \nabla \hat{\Psi} - \hat{\Psi} \nabla \Phi_f^* \}$, and its volume integral can be transformed to a surface integral using the divergence theorem. By using Eq. (2), the left-hand side of Eq. (5) may be shown to be equal to the partial photoionization amplitude [24, 25],

$$\langle \Psi_f^- | D | \Psi_0 \rangle_{\mathcal{V}} \equiv \langle \Phi_f | D | \Psi_0 \rangle_{\mathcal{V}} + \langle \Phi_f | V_f G^+(E) D | \Psi_0 \rangle_{\mathcal{V}}. \quad (6)$$

Here, $G^+(E) = (E - H + i0^+)^{-1}$ is used for retarded Green's operator. The final result thus reads:

$$\langle \Psi_f^- | D | \Psi_0 \rangle_{\mathcal{V}} = \frac{1}{2} \int_{\partial\mathcal{V}} dS \cdot \{ \Phi_f^* \nabla \hat{\Psi} - \hat{\Psi} \nabla \Phi_f^* \}, \quad (7)$$

where $\partial\mathcal{V}$ denotes the boundary of \mathcal{V} .

In the case of a one-electron target ($N = 1$), integration volume \mathcal{V} may be taken to be a sphere with radius r_0 . Let $P_f(r)$ denote the radial function of Φ_f , which describes a specific ionization channel (partial wave), and $\hat{P}(r)$ the radial function associated with the corresponding partial wave of $\hat{\Psi}$. In this case, the surface integral is proportional to Wronskian $\mathcal{W}\{P_f^*(r), \hat{P}(r)\}_{r=r_0}$, where

$$\mathcal{W}\{f(r), g(r)\}_{r=r_0} = \{f(r)g'(r) - f'(r)g(r)\}_{r=r_0}. \quad (8)$$

An elegant way of finding a solution of Eq. (2) satisfying the outgoing-wave boundary condition is to use exterior complex scaling (ECS) [8]. The ECS method is based on the complex transformation of radial coordinates,

$$R(r) = \begin{cases} r & ; r \leq R_0 \\ R_0 + (r - R_0)e^{i\vartheta} & ; r > R_0 \end{cases}, \quad (9)$$

where ϑ and R_0 are the scaling angle and radius. When ECS is used, volume \mathcal{V} is expected to lie inside the non-scaled region of space. For a one-electron atom, the latter holds when $r_0 < R_0$.

As an example, let us examine ionization of a hydrogen-like atom with nuclear charge Z . Since the electron moves in a pure Coulomb potential, we set $V_f = 0$

and $H = H_f = \mathbf{p}^2/2 - Z/r$, where $\mathbf{p} = -i\nabla$ is the electron momentum operator. Channel wave function $\Psi_f = \Phi_f$ in this case describes the chosen partial electron wave with orbital angular momentum ℓ , its projection on the quantization axis m , and energy $E = k^2/2$:

$$\Phi_f(\mathbf{r}) = \frac{P_f(r)}{r} Y_{\ell m}(\hat{\mathbf{r}}), \quad (10)$$

$$P_f(r) = \sqrt{\frac{2}{\pi k}} i^\ell e^{-i\eta_\ell(k)} F_\ell(k; r). \quad (11)$$

Here, $\hat{\mathbf{r}} = \mathbf{r}/r$, $F_\ell(k; r)$ is the regular Coulomb function for charge $Z_c = Z$, $\eta_\ell(k) = \arg \Gamma(\ell + 1 - iZ_c/k)$ the Coulomb phase shift, and $Y_{\ell m}(\hat{\mathbf{r}})$ the spherical harmonic [26]. Let us write the corresponding spherical wave of $\hat{\Psi}(\mathbf{r})$ as $r^{-1} \hat{P}(r) Y_{\ell m}(\hat{\mathbf{r}})$. As can be seen from Eqs. (7) and (8), the partial ionization amplitude is equal to:

$$\mathcal{B}_\gamma = \frac{1}{2} \sqrt{\frac{2}{\pi k}} i^{-\ell} e^{i\eta_\ell(k)} \mathcal{W}\{F_\ell(k; r), \hat{P}(r)\}_{r=r_0}, \quad (12)$$

where $\gamma = (\ell, m)$ has been used. In a converged ECS calculation, the solution of the driven Schrödinger equation for $r < R_0$ does not depend on the scaling angle (see Ref. [8] and the references cited therein). Since, furthermore, integration volume \mathcal{V} lies in the nonscaled spatial region ($r_0 < R_0$), nonscaled channel wave functions are used to calculate ionization amplitudes. As an alternative to Eq. (12), the amplitude may also be calculated as:

$$\mathcal{B}_\gamma = \frac{1}{4} \sqrt{\frac{2}{\pi k}} i^{-\ell} \mathcal{W}\{H_\ell^*(k; r), \hat{P}(r)\}_{r=r_0}, \quad (13)$$

where we have taken into account that far away from the origin, $\hat{P}(r)$ behaves as an outgoing Coulomb wave: the asymptotic form of $\hat{P}(r)$ is

$$\hat{P}(r) \sim \mathcal{A}_\gamma H_\ell(k; r) = i^{\ell-1} \sqrt{\frac{2\pi}{k}} \mathcal{B}_\gamma H_\ell(k; r), \quad (14)$$

where $H_\ell(k; r) = \exp\{-i\eta_\ell(k)\} \{F_\ell(k; r) + iG_\ell(k; r)\}$. The regular and irregular Coulomb functions behave asymptotically as $F_\ell(k; r) \sim \sin \theta_\ell^c(k; r)$ and $G_\ell(k; r) \sim -\cos \theta_\ell^c(k; r)$, where $\theta_\ell^c(k; r) = kr - \ell\pi/2 + (Z_c/k) \ln(2kr) + \eta_\ell(k)$ [24, 26]. Equations (12) and (13) can also be obtained directly from Eq. (14) if one takes into account that $\mathcal{W}\{F_\ell, H_\ell\} = ik \exp(-i\eta_\ell)$ and $\mathcal{W}\{H_\ell^*, H_\ell\} = 2ik$ [26]. Finally, the corresponding partial ionization cross section reads:

$$\sigma_\gamma(\omega) = \frac{4\pi^2}{c} g_\omega |\mathcal{B}_\gamma|^2 = \frac{2\pi}{c} g_\omega k |\mathcal{A}_\gamma|^2, \quad (15)$$

where $c = \alpha^{-1} \approx 137.036$ is the speed of light in vacuum, and $g_\omega = \omega$ or $g_\omega = \omega^{-1}$ for the length or velocity form of the dipole operator, respectively.

As our next example, let us consider a two-electron atom, e.g., the helium atom ($N = Z = 2$). In this case, single-ionization channels are specified by the quantum

numbers of the bound atomic core (n_a and ℓ_a), the orbital angular momentum of the continuum electron (ℓ), and the total angular momentum, spin, and the corresponding projections (L, M_L, S, M_S). Since at large radii, nuclear charge Z is screened by the charge of the core electron, we may write the channel Hamiltonian as

$$H_f = \frac{\mathbf{p}_1^2}{2} + \frac{\mathbf{p}_2^2}{2} - \frac{Z}{r_1} - \frac{Z}{r_2} + \frac{1}{r_>}, \quad (16)$$

where \mathbf{p}_1 and \mathbf{p}_2 are the electron momentum operators, r_1 and r_2 the radial electron coordinates, and $r_> = \max\{r_1, r_2\}$. We can then calculate the channel wave functions (Φ_f) by solving Eq. (1) in the subspace of coupled two-electron basis functions with a fixed, hydrogen-like core (n_a, ℓ_a), and for fixed ℓ, L, M_L, S , and M_S . At energy $E = I_{n_a \ell_a} + k^2/2$, which lies above ionization threshold $I_{n_a \ell_a}$, the asymptotic form of the radial function associated with channel $\gamma = (n_a, \ell_a, \ell, L, M_L, S, M_S)$ of Φ_f is written as:

$$F_\gamma^0(k; r) \sim \cos \delta_\gamma^0 F_\ell(k; r) - \sin \delta_\gamma^0 G_\ell(k; r), \quad (17)$$

where $F_\ell(k; r)$ and $G_\ell(k; r)$ are the Coulomb functions for a screened Coulomb potential ($Z_c = Z - 1$). At large r , where the effect of V_f dies out, radial function $\hat{P}(r)$ corresponding to channel γ in $\hat{\Psi}(\mathbf{r})$ behaves as described by Eq. (14). The calculation of \hat{P} is discussed in more detail in Appendix A. The partial ionization amplitude is thus calculated as:

$$\mathcal{B}_\gamma = \frac{1}{2} \sqrt{\frac{2}{\pi k}} i^{-\ell} e^{i\eta_\ell(k)} e^{i\delta_\gamma^0} \mathcal{W}\{F_\gamma^0(k; r), \hat{P}(r)\}_{r=r_0}. \quad (18)$$

An additional phase factor has been added to account for the phase shift due to the part of the short-range potential which has been accounted for in Φ_f .

While formally correct, the calculation of $F_\gamma^0(k; r)$ represents an unnecessary step. Instead of using Eq. (18), a more direct approach is to simply use unmodified Eq. (12) or Eq. (13) for $Z_c = Z - 1$ to extract the partial amplitude. This can be seen if one takes into account that r_0 is large enough, so that the asymptotic form of $F_\gamma^0(k; r)$ [Eq. (17)] can be used in Eq. (18). Note, however, that in either case, the explicit evaluation of the matrix elements of V_f is completely avoided; the latter are only needed to solve Eq. (2).

B. Two- and multiphoton ionization

We expect that the procedure described in Section II A can be generalized to the case of two-photon ionization by solving a set of driven Schrödinger equations,

$$(E_1 - H) \hat{\Psi}_1 = D \Psi_0, \quad (19)$$

$$(E_2 - H) \hat{\Psi}_2 = D \hat{\Psi}_1, \quad (20)$$

where $E_1 = E_0 + \omega$ and $E_2 = E_0 + 2\omega$. Equations (12) and (13) could then be used to extract partial ionization

amplitudes from the second-order solution ($\hat{\Psi}_2$). This procedure works as long as E_1 lies below the ionization threshold, but fails in the case of the above-threshold ionization (ATI). The reason for this is that for energies above the ionization threshold, the magnitude of the driving term in Eq. (20) does not become negligibly small near $r = r_0$, and a finite integration volume can not be used in the same way as for one-photon ionization of the atom in a bound initial state. In the case of double ionization, this problem has been addressed by replacing E_1 with $E_1 + i\beta$ ($\beta > 0$) in Eq. (19) [11, 22, 23], which results in an exponentially damped ($\sim e^{-\beta r}$) driving term in Eq. (20). Ionization amplitudes and cross sections are then calculated by extrapolating the results to $\beta \rightarrow 0^+$. However, when the energy in the intermediate step (E_1) lies close to a resonance state, the effect of the artificial damping can not be completely reversed by the numerical limiting procedure, and the magnitude of the extracted amplitude is too low.

Below we describe an alternative method which can also be used to treat resonance-enhanced photoionization. We explain its principles on the case of a one-electron atom, but keep in mind that it may also be used with few-electron atoms. Henceforth, we limit our attention to the dipole operator in the velocity form, $D = \hat{e} \cdot \mathbf{p}$, where \hat{e} is the polarization of the incident light.

In the case of ATI, the second step of the two-photon absorption process describes a continuum-continuum (CC) transition. The corresponding dipole matrix element is seen to be strongly peaked at $E_2 = E_1$ (the *on-shell approximation*) [27, 28]:

$$\langle \mathbf{k}_2 | \hat{e} \cdot \mathbf{p} | \mathbf{k}_1 \rangle \sim \delta(\mathbf{k}_2 - \mathbf{k}_1) \propto \delta(E_2 - E_1), \quad (21)$$

where \mathbf{k}_1 and \mathbf{k}_2 are the wave vectors (momenta) of the intermediate- and final-state Coulomb waves. In Eq. (21), we have used the relations $E_1 = k_1^2/2$ and $E_2 = k_2^2/2$. While Eq. (21) is exact for plane waves, it is approximately also valid for continuum states of a hydrogen-like atom (i.e., for Coulomb waves) [28]. We therefore expect that at large r , radial function $\hat{P}(r)$ associated with channel $\gamma = (\ell, m)$ of $\hat{\Psi}$ can be written as a superposition of two Coulomb waves with discrete wave numbers: $k_1 = \sqrt{2E_1}$ and $k_2 = \sqrt{2E_2}$. The latter describes the Coulomb partial wave with the expected energy of the photoelectron in the final-state, as in the case of a one-photon process. The former, however, is a direct consequence of the “mapping” of energy E_1 onto the second-order solution, which is described by Eq. (21). In Fig. 1, we show the radial function for channel $(\ell, m) = (2, 0)$ and $\omega = 1$ a.u. ($\hbar\omega \approx 27.2114$ eV), which has been calculated using Eq. (20) for the hydrogen atom driven by linearly polarized light with \hat{e} aligned along the z axis. Except near $r = 0$, where the Coulomb functions describing outgoing waves are singular, the characteristic beat-like pattern of $\hat{P}(r)$ is completely reproduced with a superposition of a pair of outgoing Coulomb waves with wave numbers equal to $k_1 = 1$ and $k_2 = \sqrt{3}$:

$$\hat{P}(r) \sim \mathcal{A}_1 H_\ell(k_1; r) + \mathcal{A}_2 H_\ell(k_2; r). \quad (22)$$

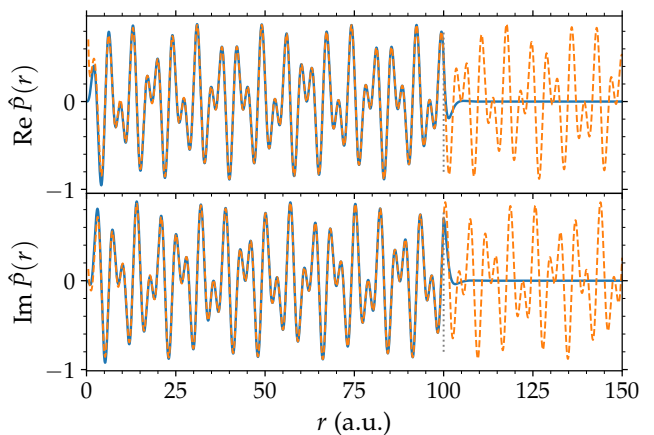


FIG. 1. Real and imaginary part of $\hat{P}(r)$ for channel $(\ell, m) = (2, 0)$ for two-photon above-threshold ionization of the hydrogen atom. The photon energy is $\omega = 1$ a.u., and the light is linearly polarized along the z axis. The scaled region of space starts at $R_0 = 100$. (marked with dotted vertical lines). The result of a least-squares fit with Coulomb functions with $k_1 = \sqrt{2E_1} = 1$ and $k_2 = \sqrt{2E_2} = \sqrt{3}$ (see text) is plotted with dashed lines for comparison (the plot has been extended beyond R_0 for clarity).

When the velocity form of the dipole operator is used ($D = \hat{e} \cdot \mathbf{p}_1 + \dots + \hat{e} \cdot \mathbf{p}_N$), a relation similar to Eq. (21) may be seen to hold also in the case of a two- or many-electron atom for CC transitions with initial and final continuum states associated with the same parent ion [29]. In other cases, like for the He atom, a similar relation may also be written when the transition occurs in the atomic core [12, 27, 30]. When the core has a complex electronic structure, several ionization channels may be open in the intermediate step, and the number of terms (different Coulomb waves) in the superposition [Eq. (22)] may be higher.

We finally arrive at the gist of the present method. We assume that at large radii, $\hat{P}(r)$ — the radial function associated with channel γ — can be written as a sum of n Coulomb waves with fixed wave numbers k_1, \dots, k_n ,

$$\hat{P}(r) \sim \sum_{q=1}^n \mathcal{A}_{\gamma,q} H_\ell(k_q; r). \quad (23)$$

In Eq. (23), k_1, \dots, k_{n-1} correspond to the open channels in the intermediate step (energy $E_1 = I_j + k_j^2/2$, $j = 1, \dots, n-1$, where I_j denotes the appropriate ionization threshold), and k_n corresponds to the chosen final-state channel (energy $E_2 = I_n + k_n^2/2$). Although Eqs. (12) and (13) can not be used directly, we may extract the ionization amplitude for channel γ ($\mathcal{A}_{\gamma,n}$) in a straightforward way. We first calculate the Wronskian of the left- and right-hand side of Eq. (23) in m radial points, which lie in the asymptotic region: $r_p < R_0$, $p = 1, \dots, m$. We define vectors $\mathbf{x} = (\mathcal{A}_{\gamma,1}, \dots, \mathcal{A}_{\gamma,n})$ and $\mathbf{b} = (b_1, \dots, b_m)$

and matrix \mathcal{M} with matrix elements \mathcal{M}_{pq} , where

$$\mathcal{M}_{pq} = \mathcal{W}\{F_\ell(k_n; r), H_\ell(k_q; r)\}_{r=r_p}, \quad (24)$$

$$b_p = \mathcal{W}\{F_\ell(k_n; r), \hat{P}(r)\}_{r=r_p}. \quad (25)$$

Alternatively, F_ℓ in Eqs. (24) and (25) may be replaced by H_ℓ^* . In the present approach, we use Wronskians to avoid accidental zeros between model functions H_ℓ at the chosen points, which can be frequent due to their oscillatory nature, and in this way increase the stability and usability of the method. We consider this approach to be a natural extension of the procedure by which we treat single-photon ionization. We can then calculate coefficients $\mathcal{A}_{\gamma,q}$ by minimizing the norm of the residual, $\mathcal{M} \cdot \mathbf{x} - \mathbf{b}$. This translates to solving the normal system: $\mathcal{M}^\dagger \cdot \mathcal{M} \cdot \mathbf{x} = \mathcal{M}^\dagger \cdot \mathbf{b}$. The two-photon ionization amplitude and the corresponding generalized partial ionization cross section are then calculated as [31]:

$$\mathcal{B}_\gamma = i^{-\ell+1} \sqrt{\frac{k_n}{2\pi}} \mathcal{A}_{\gamma,n}, \quad (26)$$

$$\sigma_\gamma^{(2)}(\omega) = \frac{8\pi^3}{c^2\omega^2} |\mathcal{B}_\gamma|^2. \quad (27)$$

The above procedure can readily be extended to treat higher-order (multiphoton) ionization. In order to calculate K -photon ionization amplitudes, we solve the system of K driven Schrödinger equations,

$$(E_1 - H)\hat{\Psi}_1 = D\Phi_0, \quad (28)$$

$$(E_2 - H)\hat{\Psi}_2 = D\hat{\Psi}_1, \quad (29)$$

⋮

$$(E_K - H)\hat{\Psi}_K = D\hat{\Psi}_{K-1}, \quad (30)$$

where $E_j = E_0 + j\omega$, $j = 1, \dots, K$, and extract the channel amplitudes from $\hat{\Psi}_K$. In this case, wave numbers k_1, \dots, k_{n-1} and k_n correspond to energies E_1, \dots, E_{K-1} and E_K , respectively. The K -photon generalized ionization cross section is then calculated as [31]:

$$\sigma_\gamma^{(K)}(\omega) = 2\pi \left(\frac{2\pi}{c\omega} \right)^K |\mathcal{B}_\gamma|^2, \quad (31)$$

where the relation between $\mathcal{A}_{\gamma,n}$ and \mathcal{B}_γ is given by Eq. (26). The cross sections can be converted to SI units by multiplying the right-hand side of Eq. (31) with $a_0^{2K} t_0^{K-1}$, where $a_0 \approx 5.29177 \times 10^{-11}$ m is the Bohr radius and $t_0 \approx 2.41888 \times 10^{-17}$ s the atomic unit of time.

III. RESULTS AND DISCUSSION

A. One-electron atom

We used the method described in Section II B to calculate two-photon ionization cross sections of the ground-state hydrogen atom shown in Fig. 2(a). The partial and

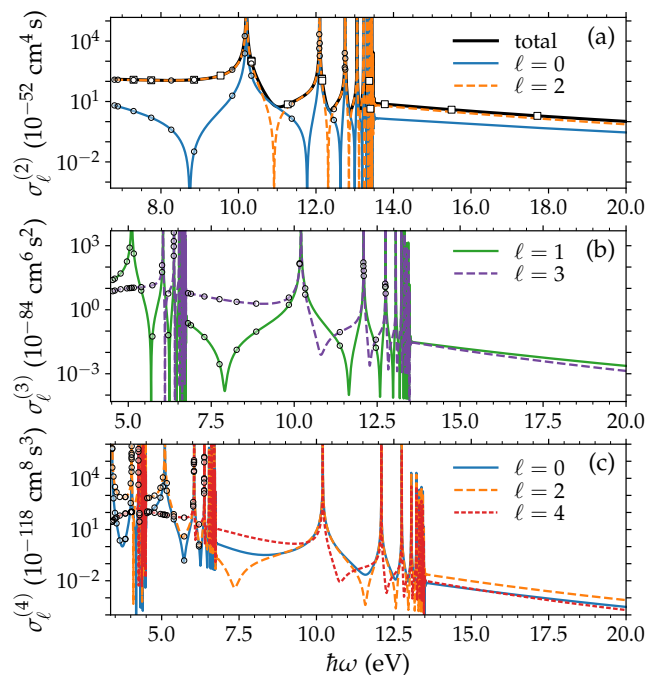


FIG. 2. Generalized two-, three-, and four-photon partial ionization cross sections of the hydrogen atom (top to bottom). The partial ionization cross sections from Ref. [32] (circles) and the total two-photon ionization cross section from Ref. [33] (squares) are plotted for comparison.

total cross sections (the sum of the $\ell = 0$ and $\ell = 2$ contributions) agree perfectly with the results of the analytic treatment of Karule [32, 33] (circles and squares). These were calculated from the tabulated values of the intensity-normalized cross section, $Q_\ell^{(2)}/I \equiv (\hbar\omega)^{-1} \sigma_\ell^{(2)}$, where I is the intensity of the linearly polarized incident light in W/cm^2 , $\hbar\omega$ the photon energy, and $\sigma_\ell^{(2)}$ the generalized cross section in $\text{cm}^4 \text{s}$. Below the ionization threshold ($\hbar\omega < 13.6$ eV), a series of peaks due to resonance-enhanced ionization through the np states is accompanied by a series of minima. Strictly speaking, without modifications, the present formalism is not suitable for photon energies close to the $1s \rightarrow np$ transition energies. When the incident photon flux is low, this can be dealt with by considering the decay and ionization of excited bound states [31]. More general alternatives in this case are, for example, to break up the overall process in steps which may not allow a perturbative description in terms of transition rates [31] or to use the non-perturbative Floquet approach [34].

In the ATI region ($\hbar\omega > 13.6$ eV), where single-photon ionization of the atom is possible, the cross sections decrease monotonically with photon energy.

The three- and four-photon ionization cross sections of the ground-state hydrogen atom are shown in panels (b) and (c) of Fig. 2. As can be seen, our results agree well with the cross sections calculated from the values of

$Q_\ell^{(K)}/I^{K-1} = (\hbar\omega)^{-K+1} \sigma_\ell^{(K)}$ tabulated in Ref. [32]. The energy thresholds at approximately 6.8 eV and 13.6 eV in Fig. 2(b) – these can be identified by the series of peaks whose positions converge to these energies – correspond to the onsets of the (2+1)-photon and (1+2)-photon ATI energy regions. Here, N in $N + W$ denotes the number of photons sufficient to ionize the atom and W stands for the number of photons absorbed above the threshold. Similarly, the thresholds at approximately 4.5 eV, 6.8 eV, and 13.6 eV mark the start of the (3+1)-, (2+2)-, and (1+3)-photon ATI energy regions in Fig. 2(c).

The cross sections shown in Fig. 2 were calculated using a radial basis of 612 modified B -spline functions [8] of order 7 for each orbital angular momentum ℓ . The radial integrals were evaluated on the ECS contour. The radial grid covered an interval up to $R_{\max} = 250$, and the radial coordinate was scaled ($\vartheta = 0.70$) beyond $R_0 = 200$. Close to the origin ($r = 0$) and for $r \gtrsim R_0$, a quadratic knot sequence was used; a linear sequence was used elsewhere. The singular value decomposition (SVD) was used to solve the normal system.

We calculated ionization amplitudes and generalized multiphoton cross sections up to order $K = 6$, but it should be noted that a calculation of cross sections of higher orders is possible. The lowest wave number which allows one to extract the ionization amplitude from $\hat{P}(r)$ is of the order of $2\pi/R_0$. In this sense, R_0 is one of the critical parameters of the extraction procedure. Another critical parameter is the number of basis functions (or, better, the density of collocation points in the radial region where the amplitudes are extracted); it determines the maximum energy (wave number) for which an accurate description of the continuum wave functions is possible [35, 36].

B. Two-electron atom

As noted, the extraction procedure can also be used to calculate multiphoton ionization amplitudes and cross sections of two- and few-electron atoms. We tested it on the case of two-, three-, and four-photon ionization of the ground-state helium atom. In Fig. 3, we plot partial ionization cross sections for linearly polarized ($\hat{e} = \hat{z}$) incident light, for which the final-state channels with $M_L = S = M_S = 0$ are accessible. The partial cross sections were calculated by summing over all the remaining channel quantum numbers but the total orbital angular momentum:

$$\sigma_L^{(K)}(\omega) = \sum_{n_a, \ell_a, \ell} \sigma_\gamma^{(K)}(\omega), \quad (32)$$

where $\gamma = (n_a, \ell_a, \ell, L, M_L, S, M_S)$ has been used. Panels (a), (c), and (e) show the below-threshold (BTI) energy region. There is generally good overall agreement between our results and the results of Saenz and Lambropoulos [37] (dashed black line), who used the time-independent perturbation theory to calculate the cross

sections. Their continuum states were calculated by solving the time-independent Schrödinger equation subject to homogeneous boundary conditions in a basis of real B -splines [36]. Since the photon energy can not be changed independently of the final-state energy, the scan over the photon energy interval was performed by varying R_{\max} (see Ref. [36] for details). While two- and three-photon cross sections from Ref. [37] match the present results rather well [panels (a) and (c)], slightly larger differences are present in the case of the four-photon partial cross sections shown in Fig. 3(e). We have checked the validity of the present results by increasing R_{\max} (R_0) and the number of basis functions. Except for the differences close to the ionization thresholds arising due to additional bound and resonance states with high principal quantum numbers, the cross sections remained unchanged. The results in the BTI region were obtained with single-particle angular momenta up to $\ell_{\max} = 6$ and with the radial functions for each of the two electrons written in a basis of 150 B -splines of order 7 per ℓ , with $R_{\max} = 170$ and $R_0 = 120$. In the ATI region, we used 85 B -splines per ℓ , $R_{\max} = 85$, and $R_0 = 50$. Partial ionization cross sections of channels with $n_a \leq 5$ were included in the sum [Eq. (32)] to obtain the cross sections in Fig. 3. In both energy regions (BTI and ATI), $\vartheta = 0.70$ was used.

Although not shown, the present results are in excellent agreement with normalized rates $w_{1s}^{(3)}/I^3 \equiv (\hbar\omega)^{-3} \sigma_{1s}^{(3)}$ reported by Proulx *et al.* [27], where I is the intensity of the incident light, $\sigma_{1s}^{(3)}$ the sum of partial three-photon cross sections for ionization leading to the helium ion in the $1s$ state ($n_a = 1, \ell_a = 0$), and $w_{1s}^{(3)}$ the corresponding ionization rate. These authors used a basis of two-electron Sturmian functions with complex radial scaling parameters and Padé extrapolation to calculate ionization amplitudes.

A practical note on the implementation of the method is in order. When some of the energies from the intermediate steps (E_1, \dots, E_{K-1}) lie above the ionization threshold, wave numbers k_1, \dots, k_{n-1} may be (approximately) degenerate or may differ by an amount too small to be “resolved” when solving the normal system. This is especially true for higher ionization thresholds. We avoid this by considering only those wave numbers which differ by more than, say, $\Delta k \sim 10^{-4}$. Furthermore, when high ionization thresholds are reached (either in the intermediate steps or the final step), bound states of the atomic core can no longer be adequately represented in a finite volume ($r \leq R_0$). We therefore choose to additionally limit the wave numbers in the intermediate steps by introducing an energy cutoff parameter. We have found the results to be stable if (approximately) equal cutoff energy for the atomic core was used to limit the intermediate- and final-state ionization channels considered in the calculation.

In Fig. 3, energy thresholds for $(N + W)$ -photon ATI may again be identified by the series of peaks converging to these energies. In the case of three-photon ionization,

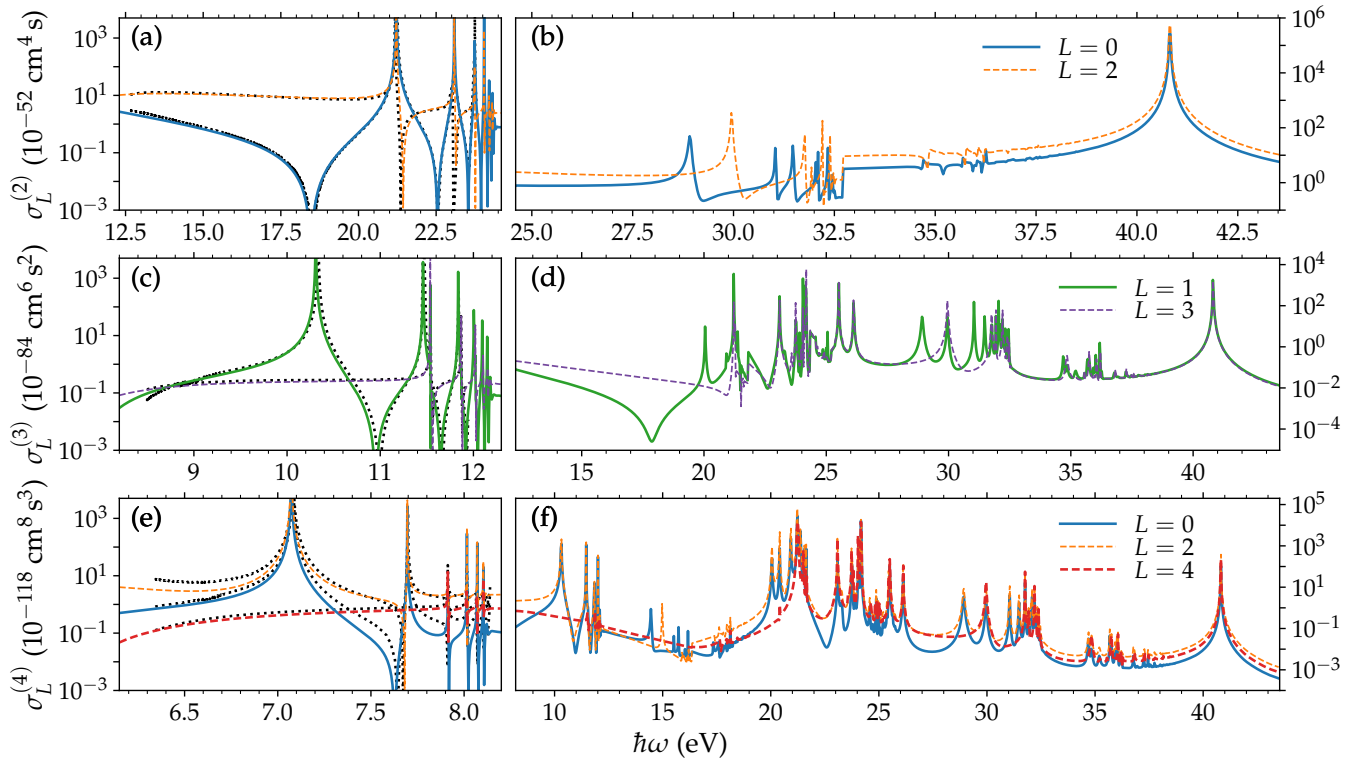


FIG. 3. Generalized two- (top), three- (middle), and four-photon (bottom) partial ionization cross sections of the helium atom. The below-threshold ionization results from Ref. [37] are plotted with dotted lines in panels (a), (c), and (e).

for example, the (2 + 1)-photon and (1 + 2)-photon ATI thresholds lie at 12.3 eV [Fig. 3(c)] and 24.6 eV [Fig. 3(d)]. In some cases, sharp jumps in $\sigma_L^{(K)}$ mark higher ionization thresholds, i.e., the thresholds for channels which describe ionization leading to the ion in an excited state, such as the $2\ell_a\epsilon_2\ell$ channels at 32.7 eV, 21.8 eV, and 16.35 eV in panels (b), (d), and (f) of Fig. 3, respectively. In Fig. 3(b), the energy thresholds of the $2\ell_a\epsilon_2\ell$ channels are preceded by a series of peaks with characteristic asymmetric profiles [38] due to the $^1S^e$ ($L = 0$) and $^1D^e$ ($L = 2$) autoionizing final states. Their asymmetric shapes are a consequence of the interference between two ionization pathways: a direct transition to the $1s\epsilon_2s$ or $1s\epsilon_2d$ continuum and an excitation to a discrete state which is followed by an electron emission. Asymmetric profiles are also present in the three- and four-photon cross sections when either the intermediate-state or the final-state continuum (or both) are resonant.

At $\hbar\omega \approx 40.8$ eV (1.5 a.u.), an enhancement in the cross sections is a signature of a shake-up like (core-excited) ionization process [12, 27, 30]. This feature is sometimes referred to as a “core-excited resonance” [30]. The enhancement is a consequence of a strong laser coupling between the $1s\epsilon_1\ell_1$ and $2p\epsilon_2\ell_2$ channels. This can be understood if we consider the following multiphoton

ionization pathway:

$$\text{g.s.} \xrightarrow{\omega} \cdots \xrightarrow{\omega} 1s\epsilon_1\ell_1 \xrightarrow{\omega} 2p\epsilon_2\ell_2 \xrightarrow{\omega} \cdots, \quad (33)$$

where g.s. stands for the helium ground state. In Eq. (33), the step written symbolically as $1s\epsilon_1\ell_1 \rightarrow 2p\epsilon_2\ell_2$ describes a CC transition, for which Eq. (21) may be used. We thus expect that the $1s\epsilon_1\ell_1$ ionization channel is strongly coupled to the $2p\epsilon_2\ell_2$ channel when $\epsilon_2\ell_2 = \epsilon_1\ell_1$, i.e., when the continuum electron acts as a spectator and the electronic transition happens in the atomic core [12, 27]. This is possible when the photon energy is approximately equal to the transition energy of the core ($\hbar\omega \approx I_{2p} - I_{1s}$). For example, in the case of two-photon ionization [Fig. 3(b)], the peak at 40.8 eV is due to the laser coupling between the $1s\epsilon_1p$ and $1s\epsilon_2p$ ionization channels (g.s. $\rightarrow 1s\epsilon_1p \rightarrow 2p\epsilon_2p$). Note that although the photon energy of 40.8 eV coincides with the $1s \rightarrow 2p$ transition energy in He^+ , Eq. (33) describes a multiphoton process in a neutral atom, i.e., it does not correspond to a two-part (“sequential”) process, in which the atom is first ionized ($\text{He} + \gamma \rightarrow \text{He}^+ 1s + e^-$) and the ground-state ion is then excited to a higher-lying state ($\text{He}^+ 1s + \gamma \rightarrow 2p$) [27]. Similar enhancements also occur at photon energies $\hbar\omega = I_{n_a} - I_{1s}$ (48.4 eV, 51.0 eV, 52.2 eV, etc.) [12, 30], where n_a denotes the principal quantum number of the excited state of the atomic core. These peaks are associated with the $1s\epsilon_1\ell \rightarrow n_a p\epsilon_2\ell$ CC

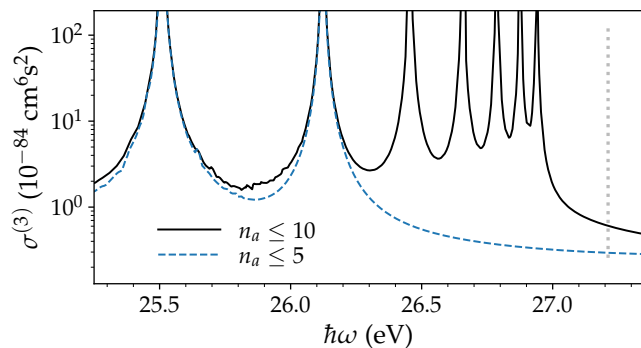


FIG. 4. Three-photon ionization cross section in the region of (1 + 2)-photon ATI. Results of two separate calculations are shown in which ionization channels with $n_a \leq 5$ (dashed blue line) and $n_a \leq 10$ (solid black line) have been included.

transitions.

As has been discussed in Ref. [12], the structure of the differential equation for the radial part of the driven Schrödinger equation describing the $2p\epsilon_2\ell_2$ channels resembles the equation of motion of a driven harmonic oscillator in which r (instead of time t) is the independent variable, and the frequency of the oscillator and the driving frequency are replaced by k_2 and k_1 , respectively. When $\hbar\omega = I_{2p} - I_{1s}$ ($k_1 = k_2$), the situation corresponds to a resonantly driven, nondamped harmonic oscillator. Exactly on resonance, the present method will fail [12]. The reason for this is that no spontaneous decay (of the core vacancy) or field-dressing effects have been included in the present formalism [30]. As in the case of bound intermediate states, this may be addressed in the framework of the (non-perturbative) Floquet formalism [34].

Photoionization which is accompanied by core excitation can also be observed at lower photon energies. One such example is (1 + 2)-photon ATI for photon energies between 25.2 eV and 27.2 eV [Fig. 3(d)]. An enlarged view of this energy interval is plotted in Fig. 4. The total three-photon cross section from two separate calculations is shown: in the first, channels with $n_a \leq 5$ have been included; in the second, $R_0 = 120$, $R_{\max} = 160$, and a larger basis set (120 B -splines per ℓ for each electron) were used to calculate partial ionization cross sections for channels with $n_a \leq 10$. As can be seen, the peak positions converge to the limit of 1 a.u. (27.2 eV), which is marked with a dotted vertical line in Fig. 4. The dominant ionization pathways underlying these enhancements are of the form g.s. $\rightarrow 1s\epsilon_1p \rightarrow 1s\epsilon_2\ell \rightarrow n_a p\epsilon_3\ell$, with $n_a \geq 4$ and $\ell = s, d$.

The present method allows one to calculate partial ionization amplitudes and cross sections also in the case of resonance-enhanced multiphoton ionization (REMPI), i.e., when the driving is resonant with a bound or a quasi-bound (resonance) state in the intermediate step. In Fig. 5, we show partial two-photon ionization cross sections in the energy region of the lowest $^1P^o$ autoionizing (doubly

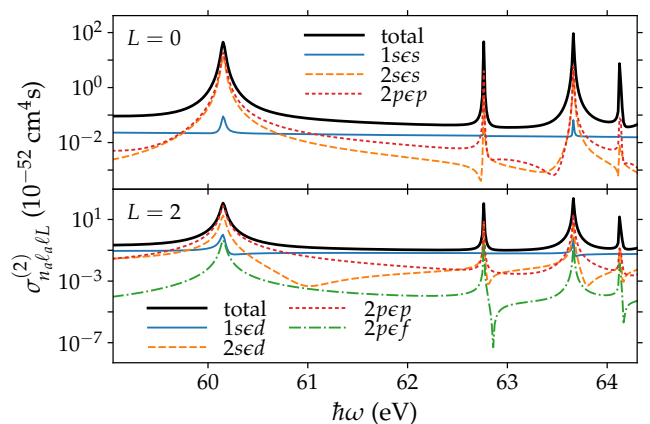


FIG. 5. Partial two-photon generalized cross sections for the $n_a \ell_a \ell L$ ionization channels in the energy region of the lowest intermediate $^1P^o$ autoionizing states: sp_2^+ , sp_3^- , sp_3^+ , and $2p3d$ (corresponding to peaks with increasing energy).

excited) resonance states: sp_2^+ , sp_3^- , sp_3^+ , and $2p3d$. We have used the notation of Cooper, Fano, and Pratts [39]. These autoionizing states, which lie below the second ionization threshold (65.4 eV), can be described primarily with the $2s2p$, $2p3s$, $2s3p$, and $2p3d$ configuration basis states. As seen in Fig. 5, as well as in Figs. 2 and 3, the method introduces no additional broadening, either below or above the ionization threshold.

C. Photoelectron angular distributions

Let us conclude the discussion by noting that it is possible to calculate photoelectron angular distributions (PADs) of helium from channel amplitudes \mathcal{B}_γ [40–42], where, as before, $\gamma = (n_a, \ell_a, \ell, L, M_L, S, M_S)$ has been used as a short-hand notation for the quantum numbers of the ionization channel. We write the angle-dependent photoelectron amplitude as:

$$\mathcal{G}_a(\mathbf{k}) = \sum_{L, \ell, m} (\ell_a, m_a; \ell, m | LM_L) \mathcal{B}_\gamma Y_{\ell m}^*(\hat{\mathbf{k}}), \quad (34)$$

where \mathbf{k} denotes the wave vector of the ejected electron, $\hat{\mathbf{k}} = \mathbf{k}/k$, m_a is the projection of the orbital angular momentum of the core and $(\ell_a, m_a; \ell, m | LM_L)$ is the Clebsch-Gordan (vector coupling) coefficient [43]. The K -photon differential cross section is then proportional to:

$$\frac{d\sigma^{(K)}}{d\Omega_{\mathbf{k}}} \propto \sum_{n_a, \ell_a, m_a} |\mathcal{G}_a(\mathbf{k})|^2. \quad (35)$$

By omitting the Clebsch-Gordan coefficient for the spin in Eq. (34), we have implicitly summed (“averaged”) over the spin quantum numbers of the target. In the present case (linearly polarized light, $\hat{\mathbf{e}} = \hat{\mathbf{z}}$), only partial waves

with $M_L = 0$ are accessible; the PADs will be axially symmetric in this case. By using the addition theorem for the spherical harmonics and the reduction formula for the $3j$ symbols [43], Eq. (35) simplifies to:

$$\sum_{n_a, \ell_a, m_a} |\mathcal{G}_a(\mathbf{k})|^2 = \sum_{j=0}^K \mathcal{N}_{2j} P_{2j}(\hat{\mathbf{e}} \cdot \hat{\mathbf{k}}), \quad (36)$$

where $P_\kappa(\hat{\mathbf{e}} \cdot \hat{\mathbf{k}}) = \sqrt{4\pi/(2\kappa+1)} Y_{\kappa,0}(\hat{\mathbf{k}})$ is the Legendre polynomial of order κ . The coefficients in Eq. (36) are:

$$\mathcal{N}_\kappa = \sum_{n_a, \ell_a} \sum_{L, L'} \sum_{\ell, \ell'} (-1)^{\kappa+\ell_a+\ell+\ell'} \hat{\kappa}^2 \hat{\ell} \hat{\ell}' \hat{L} \hat{L}' \times \begin{pmatrix} \ell & \ell' & \kappa \\ 0 & 0 & 0 \end{pmatrix} \begin{pmatrix} L & L' & \kappa \\ 0 & 0 & 0 \end{pmatrix} \left\{ \begin{matrix} L & L' & \kappa \\ \ell' & \ell & \ell_a \end{matrix} \right\} \mathcal{B}_{\gamma'} \mathcal{B}_\gamma^*. \quad (37)$$

A shorthand notation $\hat{a} = \sqrt{2a+1}$ has been introduced, and it is to be understood that indices γ and γ' are used in place of (n_a, ℓ_a, ℓ, L) and (n_a, ℓ_a, ℓ', L') . We may now define the asymmetry parameters as:

$$\beta_\kappa = \mathcal{N}_\kappa / \mathcal{N}_0, \quad (38)$$

where the expression for \mathcal{N}_0 reduces to

$$\mathcal{N}_0 = \sum_{n_a, \ell_a} \sum_{L, \ell} |\mathcal{B}_\gamma|^2 \quad (39)$$

after evaluating the $3j$ and $6j$ symbols for $\ell = \ell'$ and $L = L'$. Equations (37)–(39) agree with the analogous expressions given in Ref. [17].

In Fig. 6, we show the asymmetry parameters for two-, three-, and four-photon ionization of He. The strong variation of β_2 and β_4 in the energy region below the first ionization threshold (24.6 eV) seen in Fig. 6(a) is a consequence of two-photon ionization through the (bound) $1snp$ states. For photon energies between 30 and 40 eV, autoionizing states whose energies converge to the second ionization threshold (65.4 eV), as well as higher thresholds, can be reached; the resonant nature of the final continuum states results in a strong energy dependence of the asymmetry parameters. The parameters remain almost constant in the energy region where core-excited ionization is dominant (roughly between 40.8 eV and 54.4 eV). Finally, at even higher energies, for $\hbar\omega \gtrsim 60$ eV, the changes in the asymmetry parameters are due to two-photon ionization which proceeds through the odd-parity autoionizing states (REMPI), as shown in Fig. 5 and discussed above. The calculated asymmetry parameters are in good agreement with the results of the recent time-dependent calculation of Boll *et al.* [17], in which channel amplitudes have been extracted from the wave packet at the end of the laser pulse. Note that the main differences stem from the energy broadening due to the finite duration of the laser pulse (a 2 fs long pulse was used in Ref. [17]).

It may come as a surprise that the asymmetry parameters in Fig. 6(a) vary weakly with photon energy in the

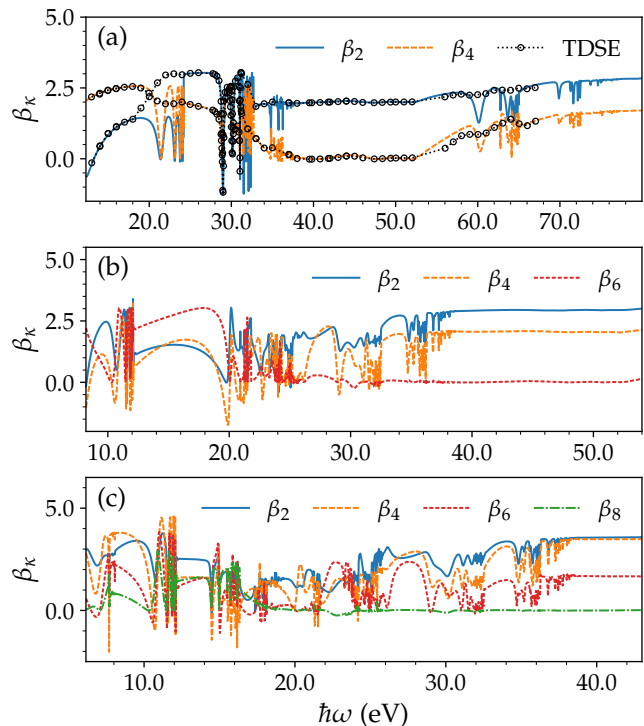


FIG. 6. Asymmetry parameters β_κ for two-, three-, and four-photon ionization of the He atom (top to bottom). The results from the time-dependent calculation (TDSE) in panel (a) are from Ref. [17].

region of core-excited ionization. It has been checked that the phase shifts of the dominant $2p\epsilon_2p$ channels are indeed smooth in this energy region. Furthermore, the values of the asymmetry parameters in this region are very close to $\beta_2 = 2$ and $\beta_4 = 0$, which describe the PADs in the case of single-photon ionization for photon energies below the second ionization threshold. This confirms that the enhancement of the cross sections is a consequence of an “external” interaction (interaction with the laser), which causes a transition inside the atomic core, but does not alter the (phases of the) final-state partial waves. Conversely, the phase shifts of the $1s\epsilon_2\ell$ ($\ell = s, d$), as well as the $2s\epsilon_2\ell$ and $2p\epsilon_2f$ channels all exhibit abrupt jumps at 40.8 eV. The latter are indicators of the coupling of these channels with the optically-accessible $2p\epsilon_2p$ channels, i.e., the jumps are a direct consequence of the electron-electron (Coulomb) coupling in the final state. Note however, that the cross sections corresponding to these channels are several orders of magnitude lower than the $2p\epsilon_2p$ cross sections.

An analogous behavior may also be seen for the asymmetry parameters in the case of three-photon [Fig. 6(b)] and four-photon [Fig. 6(c)] ionization. The parameters vary strongly when the photon energy is close to intermediate bound or resonance states or when the final-state continuum is resonant. In the region of core-excited ion-

ization, the asymmetry parameters again vary smoothly with photon energy.

IV. CONCLUSIONS

We have devised a theoretical method for the calculation of multiphoton ionization amplitudes and cross sections of few-electron atoms. The method is based on extraction of partial wave amplitudes from the scattered part of a wave function, which is obtained by solving a set of driven Schrödinger equations, and works in the case of a single electron ejection. The extraction procedure relies on a description of partial waves in terms of a small number of Coulomb waves with fixed wave numbers. We have implemented the extraction procedure in the framework of exterior complex scaling. One- and two-electron wave functions have been calculated in a basis of B -spline functions. The method has been tested by calculating partial two-, three-, and four-photon generalized cross sections of atomic hydrogen and helium, and by calculating the asymmetry parameters of photoelectron angular distributions for two-, three-, and four-photon ionization of the helium atom.

We have found the present method to be stable, robust, and its implementation to be relatively straightforward. While the method has only been tested on atomic systems, it could also be used to treat multiphoton ionization of simple molecules.

ACKNOWLEDGMENTS

We acknowledge the financial support from the Slovenian Research Agency (research programs No. P1-0112 and No. P1-0402 and research projects No. J1-8134 and No. J1-1698). This work was supported by the European COST Action CA 18222 (AttoChem). The calculations were carried out on the Olimp computer cluster at the Faculty of mathematics and physics. We thank Blaž Jensenko for his support and smooth operation of the computational facilities.

Appendix A: Calculation of radial function $\hat{P}(r)$

In this section, we provide additional details on the calculation of photoionization amplitudes for a two-electron atom. In particular, we discuss one of the possible ways of calculating radial function $\hat{P}(r)$ associated with ionization channel $\gamma = (n_a, \ell_a, \ell, L, M_L, S, M_S)$ of $\hat{\Psi}(\mathbf{r}_1, \mathbf{r}_2)$, the solution of Eq. (2). We start by expressing $\hat{\Psi}(\mathbf{r}_1, \mathbf{r}_2)$ as:

$$\hat{\Psi}(\mathbf{r}_1, \mathbf{r}_2) = \sum_{L', M_{L'}} \sum_{\alpha, \beta} y_{\alpha\beta}^{L' M_{L'}} \Phi_{\alpha\beta}^{L' M_{L'}}(\mathbf{r}_1, \mathbf{r}_2), \quad (\text{A1})$$

where $\Phi_{\alpha\beta}^{L' M_{L'}}(\mathbf{r}_1, \mathbf{r}_2)$ denotes a coupled two-electron wave function:

$$\Phi_{\alpha\beta}^{L' M_{L'}}(\mathbf{r}_1, \mathbf{r}_2) = \mathfrak{A} \frac{P_{n_\alpha \ell_\alpha}(r_1)}{r_1} \frac{P_{n_\beta \ell_\beta}(r_2)}{r_2} y_{L' M_{L'}}^{\ell_\alpha \ell_\beta}(\hat{\mathbf{r}}_1, \hat{\mathbf{r}}_2). \quad (\text{A2})$$

In Eq. (A2), $y_{L' M_{L'}}^{\ell_\alpha \ell_\beta}(\hat{\mathbf{r}}_1, \hat{\mathbf{r}}_2)$ is a bipolar harmonic [43] and \mathfrak{A} stands for the antisymmetrizing operator. (The spin parts have been omitted for brevity.) Radial functions $P_{n_\alpha \ell_\alpha}(r)$ are obtained by calculating eigen wave functions of the complex-scaled Hamiltonian operator of a one-electron atom with nuclear charge Z . These functions can be used to represent both bound and continuum states. Next, we calculate the projection by fixing the quantum numbers of the atomic core ($n_\alpha = n_a, \ell_\alpha = \ell_a$), the total angular momentum and its projection ($L' = L, M_{L'} = M_L$), and the orbital angular momentum of the “outer” electron ($\ell_\beta = \ell$):

$$\hat{\Psi}_{\alpha\ell}^{L M_L}(\mathbf{r}_1, \mathbf{r}_2) = \sum_{\beta} \Phi_{\alpha\beta}^{L M_L}(\mathbf{r}_1, \mathbf{r}_2) \langle \Phi_{\alpha\beta}^{L M_L} | \hat{\Psi} \rangle \delta_{\ell, \ell_\beta}, \quad (\text{A3})$$

where the overlap matrix element $\langle \Phi_{\alpha\beta}^{L M_L} | \hat{\Psi} \rangle$ is calculated on the ECS contour. It has been assumed above that $P_{n_a \ell_a}(r)$ describes a bound state whose wave function is contained within the nonscaled radial region, i.e., $P_{n_a \ell_a}(r)$ is taken to be negligibly small for $r > R_0$. Since wave functions $\Phi_{\alpha\beta}^{L M_L}(\mathbf{r}_1, \mathbf{r}_2)$ are diagonal in all quantum numbers, Eq. (A3) may be written as:

$$\hat{\Psi}_{\alpha\ell}^{L M_L}(\mathbf{r}_1, \mathbf{r}_2) = \sum_{\beta} \Phi_{\alpha\beta}^{L M_L}(\mathbf{r}_1, \mathbf{r}_2) y_{\alpha\beta}^{L M_L} \delta_{\ell, \ell_\beta}. \quad (\text{A4})$$

We may now immediately write the radial function describing the continuum electron in channel γ as:

$$\hat{P}(r) = \sum_{\beta} y_{\alpha\beta}^{L M_L} P_{n_\beta \ell_\beta}(r) \delta_{\ell, \ell_\beta}. \quad (\text{A5})$$

Coefficients $y_{\alpha\beta}^{L M_L}$ are calculated in the following way. We write $\hat{\Psi}$ and $\Phi_{\alpha\beta}^{L M_L}$ in a basis of two-electron functions

$$\varphi_i(\mathbf{r}_1, \mathbf{r}_2) = \mathfrak{A} \frac{B_{n_i}(r_1)}{r_1} \frac{B_{\nu_i}(r_2)}{r_2} y_{L_i M_{L_i}}^{\ell_i \lambda_i}(\hat{\mathbf{r}}_1, \hat{\mathbf{r}}_2), \quad (\text{A6})$$

where B_{n_i} and B_{ν_i} are the modified B -spline functions [8], ℓ_i and λ_i denote the orbital angular momenta of the two electrons, and L_i and M_i the total orbital angular momentum and its projection. Coefficients $y_{\alpha\beta}^{L M_L}$ are then expressed as:

$$y_{\alpha\beta}^{L M_L} = \sum_{i,j} v_i^{a\beta} \mathcal{S}_{ij} w_j, \quad (\text{A7})$$

where $\mathcal{S}_{ij} = \langle \varphi_i | \varphi_j \rangle$ is the overlap matrix element evaluated on the ECS contour, and w_j and $v_i^{a\beta}$ denote the expansion coefficients of $\hat{\Psi}$ and $\Phi_{\alpha\beta}^{L M_L}$:

$$\hat{\Psi}(\mathbf{r}_1, \mathbf{r}_2) = \sum_j w_j \varphi_j(\mathbf{r}_1, \mathbf{r}_2), \quad (\text{A8})$$

$$\Phi_{\alpha\beta}^{LM_L}(\mathbf{r}_1, \mathbf{r}_2) = \sum_i v_i^{\alpha\beta} \varphi_i(\mathbf{r}_1, \mathbf{r}_2). \quad (\text{A9})$$

-
- [1] G. Mainfray and G. Manus, *Rep. Prog. Phys.* **54**, 1333 (1991).
- [2] S. L. Chin and P. Lambropoulos, eds., *Multiphoton ionization of atoms* (Academic Press, Toronto, 1984).
- [3] C. Ott, A. Kaldun, L. Argenti, P. Raith, K. Meyer, M. Laux, Y. Zhang, A. Blättermann, S. Hagstotz, T. Ding, R. Heck, J. Madroñero, F. Martín, and T. Pfeifer, *Nature* **516**, 374 (2014).
- [4] K. C. Prince, E. Allaria, C. Callegari, R. Cucini, G. De Ninno, S. Di Mitri, B. Diviacco, E. Ferrari, P. Finetti, D. Gauthier, L. Giannessi, N. Mahne, G. Penco, O. Plekan, L. Raimondi, P. Rebernik, E. Rousset, C. Svetina, M. Trovò, M. Zangrando, M. Negro, P. Carpeggiani, M. Reduzzi, G. Sansone, A. N. Grum-Grzhimailo, E. V. Gryzlova, S. I. Strakhova, K. Bartschat, N. Douguet, J. Venzke, D. Iablonskyi, Y. Kumagai, T. Takanashi, K. Ueda, A. Fischer, M. Coreno, F. Stienkemeier, Y. Ovcharenko, T. Mazza, and M. Meyer, *Nat. Photonics* **10**, 176 (2016).
- [5] M. Žitnik, A. Mihelič, K. Bučar, M. Hrast, Ž. Barba, Š. Krušič, P. Rebernik Ribič, J. Urbančič, B. Ressel, M. Stupar, L. Poletto, M. Coreno, D. Gauthier, and G. De Ninno, *Phys. Rev. A* **99**, 053423 (2019).
- [6] G. De Ninno, J. Wätzel, P. R. Ribič, E. Allaria, M. Coreno, M. B. Danailov, C. David, A. Demidovich, M. Di Fraia, L. Giannessi, K. Hansen, Š. Krušič, M. Manfreda, M. Meyer, A. Mihelič, N. Mirian, O. Plekan, B. Ressel, B. Rösner, A. Simoncig, S. Spampinati, M. Stupar, M. Žitnik, M. Zangrando, C. Callegari, and J. Berakdar, *Nat. Photonics* **14**, 554 (2020).
- [7] D. You, K. Ueda, E. V. Gryzlova, A. N. Grum-Grzhimailo, M. M. Popova, E. I. Staroselskaya, O. Tugs, Y. Orimo, T. Sato, K. L. Ishikawa, P. A. Carpeggiani, T. Csizmadia, M. Füle, G. Sansone, P. K. Maroju, A. D’Elia, T. Mazza, M. Meyer, C. Callegari, M. Di Fraia, O. Plekan, R. Richter, L. Giannessi, E. Allaria, G. De Ninno, M. Trovò, L. Badano, B. Diviacco, G. Gaio, D. Gauthier, N. Mirian, G. Penco, P. c. v. R. Ribič, S. Spampinati, C. Spezzani, and K. C. Prince, *Phys. Rev. X* **10**, 031070 (2020).
- [8] C. W. McCurdy and F. Martín, *J. Phys. B* **37**, 917 (2004).
- [9] C. W. McCurdy, M. Baertschy, and T. N. Rescigno, *J. Phys. B* **37**, R137 (2004).
- [10] C. W. McCurdy, D. A. Horner, T. N. Rescigno, and F. Martín, *Phys. Rev. A* **69**, 032707 (2004).
- [11] D. A. Horner, F. Morales, T. N. Rescigno, F. Martín, and C. W. McCurdy, *Phys. Rev. A* **76**, 030701(R) (2007).
- [12] A. Mihelič, *Phys. Rev. A* **98**, 023409 (2018).
- [13] A. Scrinzi, *Phys. Rev. A* **81**, 053845 (2010).
- [14] A. Palacios, C. W. McCurdy, and T. N. Rescigno, *Phys. Rev. A* **76**, 043420 (2007).
- [15] A. Palacios, T. N. Rescigno, and C. W. McCurdy, *Phys. Rev. A* **77**, 032716 (2008).
- [16] A. Palacios, T. N. Rescigno, and C. W. McCurdy, *Phys. Rev. A* **79**, 033402 (2009).
- [17] D. I. R. Boll, O. A. Fojón, C. W. McCurdy, and A. Palacios, *Phys. Rev. A* **99**, 023416 (2019).
- [18] L. Tao and A. Scrinzi, *New J. Phys.* **14**, 013021 (2012).
- [19] A. Scrinzi, *New J. Phys.* **14**, 085008 (2012).
- [20] T. Sato, K. L. Ishikawa, I. Březinová, F. Lackner, S. Nagele, and J. Burgdörfer, *Phys. Rev. A* **94**, 023405 (2016).
- [21] Y. Orimo, T. Sato, A. Scrinzi, and K. L. Ishikawa, *Phys. Rev. A* **97**, 023423 (2018).
- [22] D. A. Horner, C. W. McCurdy, and T. N. Rescigno, *Phys. Rev. A* **78**, 043416 (2008).
- [23] D. A. Horner, T. N. Rescigno, and C. W. McCurdy, *Phys. Rev. A* **77**, 030703(R) (2008).
- [24] C. J. Joachain, *Quantum Collision Theory* (North-Holland, Amsterdam, 1975).
- [25] I. Adawi, *Am. J. Phys.* **32**, 211 (1964).
- [26] F. W. J. Olver, D. W. Lozier, B. R. F., and C. W. Clark, eds., *NIST Handbook of Mathematical Functions* (Cambridge University Press, New York, 2010).
- [27] D. Proulx, M. Pont, and R. Shakeshaft, *Phys. Rev. A* **49**, 1208 (1994).
- [28] C. Marante, L. Argenti, and F. Martín, *Phys. Rev. A* **90**, 012506 (2014).
- [29] A. Jiménez-Galán, F. Martín, and L. Argenti, *Phys. Rev. A* **93**, 023429 (2016).
- [30] R. Shakeshaft, *Phys. Rev. A* **76**, 063405 (2007).
- [31] P. Lambropoulos, P. Maragakis, and J. Zhang, *Phys. Rep.* **305**, 203 (1998).
- [32] E. Karule, *J. Phys. B* **21**, 1997 (1988).
- [33] E. Karule, *J. Phys. B* **11**, 441 (1978).
- [34] S.-I. Chu and D. A. Telnov, *Phys. Rep.* **390**, 1 (2004).
- [35] M. Venuti, P. Decleva, and A. Lisini, *J. Phys. B* **29**, 5315 (1996).
- [36] H. Bachau, E. Cormier, P. Decleva, J. E. Hansen, and F. Martín, *Rep. Prog. Phys.* **64**, 1815 (2001).
- [37] A. Saenz and P. Lambropoulos, *J. Phys. B* **32**, 5629 (1999).
- [38] I. Sánchez, H. Bachau, and E. Cormier, *J. Phys. B* **28**, 2367 (1995).
- [39] J. W. Cooper, U. Fano, and F. Prats, *Phys. Rev. Lett.* **10**, 518 (1963).
- [40] P. O’Keeffe, P. Bolognesi, A. Mihelič, A. Moise, R. Richter, G. Cautero, L. Stebel, R. Sergio, L. Pravica, E. Ovcharenko, P. Decleva, and L. Avaldi, *Phys. Rev. A* **82**, 052522 (2010).
- [41] P. O’Keeffe, A. Mihelič, P. Bolognesi, M. Žitnik, A. Moise, R. Richter, and L. Avaldi, *New J. Phys.* **15**, 013023 (2013).
- [42] T. Carette, J. M. Dahlström, L. Argenti, and E. Lindroth, *Phys. Rev. A* **87**, 023420 (2013).
- [43] D. M. Brink and G. R. Satchler, *Angular momentum*, 2nd ed. (Clarendon, Oxford, 1975).